

# How is the density of quasi-two-dimensional uniform dipolar quantum Bose gases affected by trap imperfections?

Thibault Bourgeois<sup>1,2</sup>, Lauriane Chomaz<sup>1,\*</sup>.

<sup>1</sup> *Physikalisches Institut, Universität Heidelberg, Im Neuenheimer Feld 226, 69120, Heidelberg, Germany.*

<sup>2</sup> *Département de Physique, Ecole Normale Supérieure, 24 rue Lhomond, 75005, Paris, France.*

(Dated: March 8, 2024)

We theoretically investigate the impact of weak perturbations of a flat potential on the density of a quasi-two-dimensional dipolar Bose gas. We use a mean-field perturbative treatment of the potential defects and derive their effects at first order in the mean-field stable regime. We first focus on defects containing a single spatial frequency and study the wavevector dependence of the density perturbation. A qualitative modification of the wavenumber dependence with the interaction parameters and a sensitivity in the excitation direction reveal the long-range and anisotropic dipolar effects. These effects are found to be most important at intermediate wavenumbers and can give rise to a local maximum in the density perturbation reminiscent of the roton mode softening and local instabilities. The dependence on the gas and interaction parameters is studied. The case of a flat potential perturbed with white noise on a certain momentum range is then examined. Here it is found that the strength perturbation becomes independent of the mean density when sufficiently large. Our study touches upon experimentally relevant issues, giving hints on how flat a uniform potential should be to achieve uniform quasi-two-dimensional dipolar Bose gases.

## I. INTRODUCTION

The achievement of quantum degeneracy in gases of atoms with large magnetic dipole moments in their electronic ground states has opened up new avenues of research in which long-range anisotropic dipole-dipole interactions (DDI) play a crucial role. In such gases, a large diversity of behaviors arises from the competition between interactions of different origins and characters (contact and dipolar) and the external potential geometry. For instance, a variety of novel many-body quantum states, liquid-like droplets, droplet crystals, and supersolids, have recently been discovered through this competition [1].

While experiments so far have relied on standard harmonic traps created by Gaussian beams, traps of different geometries may allow further exotic behaviors and new phases to emerge [2–5]. Recent major technical developments have enabled the creation of such exotic geometries in ultracold-gas experiments of alkali atoms [6] and are to be extended to the magnetic atom cases, see also ref. [7]. Yet technical limitations to the realization of the desired potential occur from e.g. unwanted optical aberrations and speckles that yield potential defects of small amplitude and varied length scales.

Speckle potentials can also be created on purpose to generate random potentials and study phenomena related to the dirty boson concept. This general concept, which first arose in the context of experiments on superfluid helium in porous media, describes the effect of impurities or disorder on a quantum assembly of interacting bosons. It has been widely studied theoretically in the case of contact interacting systems at zero and finite temperatures as well as in arbitrary dimensions, see e.g. [8–15]. The effect of unwanted potential defects can be understood from these studies. One of the most intriguing questions related to the dirty boson con-

cept, already raised by early observations in superfluid helium [16], concerns the occurrence of ordered coherent states (superfluid) despite the presence of disorder and under the competing effect of interactions. Other interesting effects regard the gas shape and its excitations, which have been for part studied in recent experiments with ultracold gases [17].

More recently, the case of dirty dipolar bosons, i.e. dipolar Bose-Einstein condensates (BEC) in presence of disorder, has also been theoretically investigated at both zero and finite temperatures in 3D [18–21] and in quasi-2D assuming transverse dipole orientation [22, 23]. However, while first-order effects have been considered in works on contact-interacting systems [11, 13], they have so far been neglected in studies of the dipolar case, assuming their cancellation over ensemble average. In this manuscript, we investigate the effect of static random potential perturbations on BECs with strong and tunable dipolar interactions competing with contact interactions, as realized by ultracold gases of magnetic atoms. We focus on perturbations of the condensate density, and due to the static nature of the potential, the dominant effects are of first order. Such static random potentials capture the impact of optical imperfections in the realization of tailorable potentials. Here we focus on the mean-field stable regime corresponding to the case of a uniform superfluid, leaving aside the vast question of the effects of potential defects on self-ordered states such as droplet crystals or supersolids. In particular, we do not include Lee-Huang-Yang corrections in the Gross-Pitaevskii equation considered [1].

The paper is organized as follows: In Sec. II we present our model of a quasi-2D dipolar BEC and calculate the first-order perturbation of the wavefunction for arbitrary potentials. The relevant energy scales and the region of mean-field stability of the atomic cloud are also studied from perturbation theory. In Sec. III, we study the ef-

fects of a purely sinusoidal perturbation of the potential. We investigate the impact of the dipolar interactions on the density perturbations through tuning the dipole and excitation directions, the relative strength of dipolar and contact interactions, and the gas parameters. Finally, in Sec. IV we consider a more realistic random potential with white noise on a certain momentum range, allowing us to extract a power law dependence of the perturbation with the density.

## II. THEORETICAL MODEL

### A. The quasi-2D dipolar Bose gas

We consider a weakly interacting quantum Bose gas confined in a small region of space. The trap is tight and harmonic along  $z$ , such that the trapping frequency  $\nu_z$  is much larger than the accessible energy scales in the gas, especially the thermal and chemical potential one. In this case, the gas populates only the harmonic ground state along  $z$ , with typical length scale  $\ell_z = \sqrt{\hbar/m\nu_z}/2\pi$ , and this direction can be integrated out of the equation of motion. The position in the transverse plane is represented by the vector  $\mathbf{r}$  and the trapping potential in this plane is arbitrary and denoted  $V(\mathbf{r})$ . The gas is described by its macroscopic in-plane ground-state wavefunction,  $\psi(\mathbf{r})$ . In presence of a generic interparticle interaction potential  $U_{\text{int}}(\mathbf{r})$ , in equilibrium, it satisfies the generalized stationary quasi-2D Gross Pitaevskii equation [24–27]:

$$\mu\psi = \left[ \frac{-\hbar^2}{2m} \Delta + V(\mathbf{r}) + \int d^3r' U_{\text{int}}(\mathbf{r} - \mathbf{r}') |\psi(\mathbf{r}')|^2 \right] \psi \quad (1)$$

Here  $\mu$  is gas chemical potential. The first term on the right-hand side of the equation is the kinetic term with  $m$  the particle mass. The second term accounts for the effect of the confining potential. The third term describes the (binary) inter-atomic interactions.

In this paper, we focus on the case where atoms interact via both contact and dipole-dipole interactions [1]. We assume the dipoles to be polarized by an external magnetic field. In this case, the three-dimensional interparticle interaction (pseudo-)potential  $U_{\text{int}}(\mathbf{R})$  can be written as:

$$U_{\text{int}}^{(3D)}(\mathbf{R}) = \frac{4\pi\hbar^2 a_s}{m} \delta(\mathbf{R}) + \frac{3\hbar^2 a_{\text{dd}}}{m} \frac{1 - 3\cos^2\theta}{|\mathbf{R}|^3} \quad (2)$$

where  $\theta$  is the angle between the dipole orientation and the interatomic axis  $\mathbf{R} = \mathbf{r} + z\mathbf{e}_z$ , and  $a_s$  and  $a_{\text{dd}}$  are the contact and dipolar length respectively. In the case of magnetic dipoles of magnetic moment  $\mu_d$ ,  $a_{\text{dd}} = \frac{m\mu_0\mu_d^2}{12\pi\hbar^2}$  with  $\mu_0$  the Bohr magneton [24–27]. We define  $\epsilon_{\text{dd}} = a_{\text{dd}}/a_s$  and  $g = \frac{4\pi\hbar^2 a_s}{m}$ .

Integrating out the  $z$  direction yields the quasi-2D interaction potential  $U_{\text{int}}(\mathbf{r})$ . This potential is conveniently

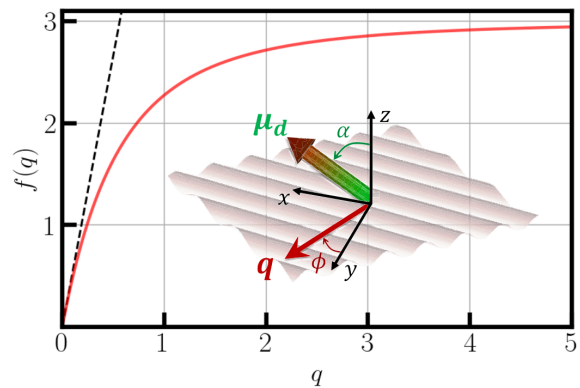


FIG. 1. **Quasi-2D dipolar system and interaction** Inset: Sketch of the geometry. The gas is strongly confined along  $z$ , yielding a quasi-2D system in the  $x, y$ -plane. The dipoles (green and red arrow) are oriented in the  $x, z$  plane and make an angle  $\alpha$  with the  $z$  axis. We typically reason in momentum space and consider a normalized wavevector  $\mathbf{q}$  (red arrow and red wave pattern in the  $x, y$  plane) making an angle  $\phi$  with the  $y$  axis. Main graph: plot of the function  $f$  (Eq. (6)). The dotted black line is the asymptotic limit  $f(q) \sim_{q \rightarrow 0} 3\sqrt{\pi}q$ .

expressed in momentum space via:

$$\tilde{U}(\mathbf{k}) = \mathcal{F}\{U_{\text{int}}(\mathbf{r})\} = \frac{g}{\sqrt{2\pi}\ell_z} [1 + \epsilon_{\text{dd}}F(\mathbf{q}, \alpha)] \quad (3)$$

with  $\mathcal{F}\{\bullet(\mathbf{r})\} = \frac{1}{(2\pi)^2} \int \bullet(\mathbf{r}) e^{i\mathbf{k}\cdot\mathbf{r}} d\mathbf{r}$  the 2D Fourier transform operator,  $\mathbf{k}$  the conjugate coordinate to  $\mathbf{r}$ ,  $\mathbf{q} = \mathbf{k}\ell_z/\sqrt{2}$  the adimensionned momentum, and  $\alpha$  the angle between the dipole and the  $z$ -axis. The geometry considered is illustrated in Figure 1 inset. Assuming that the dipoles are in the  $(x, z)$ -plane, the function  $F(\mathbf{q}, \alpha)$  is:

$$F(\mathbf{q}, \alpha) = F_{\parallel}(\mathbf{q}) \sin^2 \alpha + F_{\perp}(\mathbf{q}) \cos^2 \alpha, \quad (4)$$

$$F_{\parallel}(\mathbf{q}) = -1 + f(q) \sin^2 \phi, \quad F_{\perp}(\mathbf{q}) = 2 - f(q), \quad (5)$$

with  $\phi$  the angle between  $\mathbf{k}$  and the  $y$  axis and  $q$  the norm of  $\mathbf{q}$ . The momentum dependence is encompassed by the function

$$f(q) = 3\sqrt{\pi}q e^{q^2} \text{erfc}(q) \quad (6)$$

with  $\text{erfc}$  the complementary error function. This function is positive for all  $q \in \mathbb{R}^+$  and its asymptotic behaviors are  $f(q) \sim_{q \rightarrow 0} 3\sqrt{\pi}q$  and  $f(q) \sim_{q \rightarrow \infty} 3$ . The function  $f(q)$  is plotted in Figure 1.

We can also isolate the momentum dependence in  $F(\mathbf{q}, \alpha)$  as

$$F(\mathbf{q}, \alpha) = (3 \cos^2 \alpha - 1) + f(q) [\sin^2 \alpha \sin^2 \phi - \cos^2 \alpha], \quad (7)$$

or its angular dependence as

$$F(\mathbf{q}, \alpha) = (-1 + f(q) \sin^2 \phi) + \cos^2 \alpha (3 - f(q) [\sin^2 \phi + 1]). \quad (8)$$

Interestingly,  $F(\mathbf{q}, \alpha)$  is always decreasing with  $q$  for  $\phi = 0$  (excitation perpendicular to the dipole plane), while for  $\phi > 0$ , the variation of  $F(\mathbf{q}, \alpha)$  with  $q$  changes direction for  $\alpha$  above a certain value. In the case of  $\phi = \pi/2$ , the change occurs at  $\alpha = \pi/4$ . This stems from the fact that, in the case of long-range interactions, the interaction cost of a density modulation of wavevector  $\mathbf{k} \neq 0$  has contributions not only from interactions in the  $\mathbf{k}$  direction, but also from interactions in the direction transverse to  $\mathbf{k}$ , and the weight of the latter increases with  $q$ . This transverse contribution is more or less attractive than the longitudinal contribution depending on the orientation of the dipoles compared to  $\mathbf{k}$ , thus fixing the sign of the variations with  $q$ . The variations of  $F$  with  $\mathbf{k}$  will be crucial for our later study. Furthermore, we note that the asymptotic behaviors of  $f(q)$  yield the following limits for the interaction potential itself:

$$\tilde{U}(\mathbf{k} \rightarrow 0) = \frac{g [1 + \epsilon_{dd}(3 \cos^2 \alpha - 1)]}{\sqrt{2\pi}\ell_z}, \quad (9)$$

$$\tilde{U}(\mathbf{k} \rightarrow \infty) = \frac{g [1 + \epsilon_{dd}(3 \sin^2 \alpha \sin^2 \phi - 1)]}{\sqrt{2\pi}\ell_z} \quad (10)$$

### B. Zeroth- and first-order perturbation theory — condensate density and its fluctuations

In the following, we consider a confinement potential  $V(\mathbf{r}) = V_0(\mathbf{r}) + \delta V(\mathbf{r})$  being a uniform box potential  $V_0(\mathbf{r})$  of size  $L$  perturbed by potential defect  $\delta V(\mathbf{r})$ , with  $\int \delta V(\mathbf{r}) d\mathbf{r} = 0$ .

First, we assume that the typical size of the trap  $L$  is much larger than the healing length  $\xi = \sqrt{\hbar^2/m\mu}$ , defining the characteristic length scale over which the wavefunction can cancel,  $L \gg \xi$ . In this case, in the absence of potential perturbation  $\delta V = 0$ , the 2D condensate wavefunction can be assumed to be uniform  $\psi = \psi_0 = \sqrt{n_0}$  with  $n_0 = N/L^2$  the 2D atomic density and  $N$  the atom number. Using Eq. (1) and Eq. (9), the chemical potential reads

$$\mu = \tilde{U}(0)n_0 = \frac{gn_0}{\sqrt{2\pi}\ell_z} [1 + \epsilon_{dd}(3 \cos^2 \alpha - 1)] \quad (11)$$

We now consider the effect of the potential defects  $\delta V$  in perturbation and consider the first order expansion  $\psi(\mathbf{r}) = \psi_0 + \psi^{(1)}(\mathbf{r})$ , with  $\int \psi^{(1)}(\mathbf{r}) d\mathbf{r} = 0$ . In the following, we prefer reasoning in momentum space and write  $\psi(\mathbf{k}) = \psi_0 \delta(k) + \tilde{\psi}^{(1)}(\mathbf{k})$  with  $\tilde{\psi}^{(1)}(\mathbf{k}) = \mathcal{F}\{\psi^{(1)}(\mathbf{r})\}$  and  $\tilde{\psi}^{(1)}(0) = 0$ . We also characterize the potential defect  $\delta V$  via its Fourier components  $\delta\tilde{V}(\mathbf{k}) = \mathcal{F}\{\delta V(\mathbf{r})\}$ .

Expanding the Gross-Pitaevskii Eq. (1) to first order using Eq. (3) yields:

$$\tilde{\psi}^{(1)}(\mathbf{k}) = \frac{-\sqrt{n_0}\delta\tilde{V}(\mathbf{k})}{\frac{\hbar^2\mathbf{k}^2}{2m} + 2n_0\tilde{U}(\mathbf{k})}, \quad (12)$$

see also ref. [18]. From this, we deduce the perturbed

density at first order via:

$$n(\mathbf{r}) = |\psi(\mathbf{r})|^2 = n_0 + 2\sqrt{n_0} \int \psi^{(1)}(\mathbf{k}) e^{-i\mathbf{k}\cdot\mathbf{r}} d\mathbf{r} \quad (13)$$

This reads as  $n = n_0 + n^{(1)}(\mathbf{r})$  with  $n^{(1)}$  the first order correction in the density, from which the momentum dependence is easily expressed as

$$\tilde{n}^{(1)}(\mathbf{k}) = \mathcal{F}\{n^{(1)}(\mathbf{r})\} = \frac{-2n_0\delta\tilde{V}(\mathbf{k})}{\frac{\hbar^2\mathbf{k}^2}{2m} + 2n_0\tilde{U}(\mathbf{k})} \quad (14)$$

This equation sets the basic framework for our study.

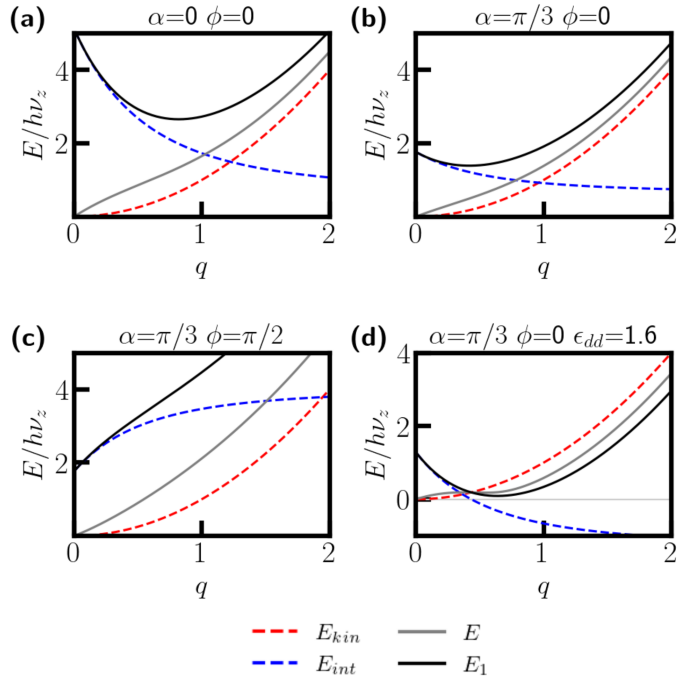


FIG. 2. **Energy scales.** Values of the different energies as a function of  $q$  for different angles  $(\alpha, \phi)$  and values of  $\epsilon_{dd}$ . The red dashed line is the kinetic term  $E_{kin}(\mathbf{k})$ , the blue dashed line is the interaction term  $E_{int}(\mathbf{k})$ . The black curve is the total energy  $E_1(\mathbf{k})$  while the gray one is the Bogoliubov perturbation  $E(\mathbf{k})$ . If not specified,  $\epsilon_{dd} = 0.7$ . The other parameters used are  $\nu_z = 1$  kHz,  $n_0 = 125 \mu\text{m}^{-2}$ ,  $m = 164$  a.u. and  $a_s = 130 a_0$ .

### C. Energy scale analysis from perturbation theory

The denominator of the right-hand side of the fundamental equation (14) is a characteristic energy scale associated with the momentum  $\mathbf{k}$ , which we denote

$$E_1(\mathbf{k}) = \frac{\hbar^2\mathbf{k}^2}{2m} + 2n_0\tilde{U}(\mathbf{k}). \quad (15)$$

It consists of the sum of a kinetic and an interaction term,  $E_{kin} = \hbar^2\mathbf{k}^2/2m$  and  $E_{int} = 2n_0\tilde{U}(\mathbf{k})$ , respectively. It is

interesting to note that this energy scale differs from the elementary excitation energy of the unperturbed condensate which is calculated from second-order Bogoliubov theory and is given by [1, 24]:

$$E(\mathbf{k}) = \sqrt{\frac{\hbar^2 \mathbf{k}^2}{2m} \left( \frac{\hbar^2 \mathbf{k}^2}{2m} + 2n_0 \tilde{U}(\mathbf{k}) \right)}. \quad (16)$$

In particular,  $E(\mathbf{k})$  has a larger contribution from the kinetic term than  $E_1(\mathbf{k})$  and reads  $E(\mathbf{k}) = \sqrt{E_{\text{kin}}(\mathbf{k})E_1(\mathbf{k})}$ .

In Figure 2 we represent the different energy scales  $E_{\text{kin}}$ ,  $E_{\text{int}}$ ,  $E_1$  and  $E$ , as a function of  $q$  in a few exemplary situations. We note that depending on the choice of angles  $(\alpha, \phi)$  the variations of  $E_{\text{int}}$  with  $q$  may change sign. Here we see that  $E_{\text{int}}$  decreases with  $q$  for  $\phi = 0$  (a,b,d) and increases with  $q$  for  $(\alpha = \pi/3, \phi = \pi/2)$  (c), see also previous discussion in Sec. II A. At large  $q$ , we observe that  $E_{\text{kin}}$  tends to dominate over  $E_{\text{int}}$  and both  $E_1$  and  $E$  tend to follow the variations of  $E_{\text{kin}}$ . Instead, at small and intermediate momenta, the variations of  $E_1$  and  $E$  are clearly distinct.

At small momenta, we observe that  $E_1$  tends to follow the behavior of  $E_{\text{int}}$ , which dominates over  $E_{\text{kin}}$ . Therefore  $E_1$  takes a finite value at zero momentum that depends on the interaction and gas parameters, and it varies at small momenta in a similar manner as  $E_{\text{int}}$ , i.e. with a slope dictated by the choice of angles  $(\alpha, \phi)$ . For choices such that  $E_{\text{int}}$  initially decreases with  $q$ ,  $E_1$  presents a minimum at finite momentum. Instead, the Bogoliubov dispersion  $E$  always tends to zero at  $q \rightarrow 0$  and grows linearly at small momenta, following a phononic behavior. Therefore, even if  $E_1$  is non-monotonous in a wide range of situations,  $E$  typically is monotonous. This is due to the enhanced contribution of the kinetic term in Eq. (16).

Yet, in some cases, we observe that  $E$  becomes non-monotonous, forming a local maximum and a local minimum at finite  $q$ , as observed in (d). This corresponds to the occurrence of the celebrated maxon-roton dispersion relation under the effect of dipolar interactions and strong transverse confinement [1, 24, 28, 29]. While the softening of a roton mode is a signature of the special dependence of the interaction energy with  $q$  and of its competition with the kinetic energy, we note that signatures of this competition are much more obvious in the behavior of  $E_1$  itself. Based on Eq. (14), we expect similar strong signatures on the density perturbations induced by potential defects as will be discussed later in this manuscript (see Sec. III A).

#### D. Mean-field stability analysis from perturbation theory

In analyzing the behavior of the first-order density perturbation  $\tilde{n}^{(1)}$  and the energy scale  $E_1(\mathbf{k})$  coming at its denominator, we observe a peculiar behav-

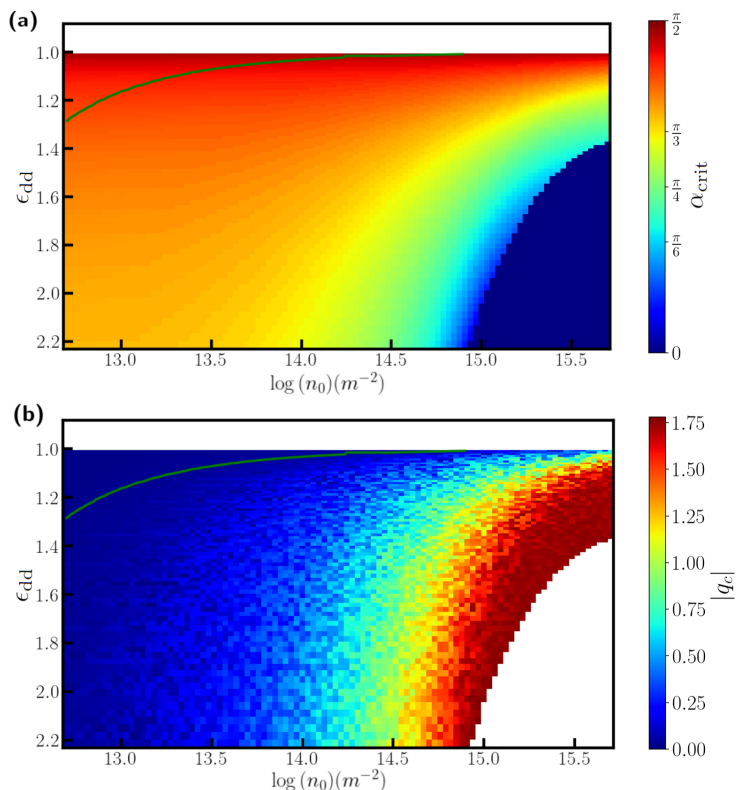


FIG. 3. **Identification of instability.** (a) Values of  $\alpha_{\text{crit}}$ , the smallest angle  $\alpha$  at which there exists one unstable momentum  $E_1(\mathbf{k}) = 0$ , as a function of the interaction parameter  $\epsilon_{\text{dd}}$  and the mean 2D density  $n_0$ . The white region for  $\epsilon_{\text{dd}} < 1$  is the region where no instability occurs. (b) Norm of the unstable momentum  $\mathbf{q}_c$  at  $\alpha = \alpha_{\text{crit}}$ . The green line shows the boundary of the region where the instability occurs at  $\mathbf{q}_c = 0$ . The other parameters are fixed to  $\nu_z = 1$  kHz and the gas parameters  $m = 134$  a.u.,  $a_{\text{dd}} = 133 a_0$ , while the changes of  $\epsilon_{\text{dd}}$  are made by varying  $a_s$ .

ior. Under some circumstances,  $E_1$  may vanish (see Eqs. (15),(7),(3)), yielding divergingly large perturbations in Eq. (14). This regime, in which perturbation theory breaks down, corresponds to a well-known effect in mean-field theory, namely that of mean-field instability [1, 24, 27, 30, 31]. In dipolar gases in particular, this effect has been widely studied due to its dependence on the interaction parameters and on the gas geometry [1, 27, 30, 31]. There it was found that the instability can either be of global character, driven by the softening of  $\mathbf{k} = 0$  excitation; or of local character, driven by the softening of roton-like excitation at finite momenta.

In this subsection, we investigate the (in)stability condition through the analysis of the behavior of  $E_1(\mathbf{k})$  with the aim to identify the regime of validity of the theory of Sec. II B. The instability is identified by the existence of a vector  $\mathbf{k}$  for which  $E_1(\mathbf{k})$  vanishes. We find that for a given set of gas and interaction parameters  $(\epsilon_{\text{dd}}, a_s, n_0, \ell_z)$ , the gas is unstable for all dipole orientations with  $\alpha > \alpha_{\text{crit}}$  where  $\alpha_{\text{crit}}$  is a critical angle depending on the

above parameters.

Figure 3 (a) shows the value of the critical angle  $\alpha_{\text{crit}}$  as a function of  $\epsilon_{\text{dd}}$  and the 2D atomic density  $n_0$ . First, we observe that the gas is always stable if  $\epsilon_{\text{dd}} < 1$ , that is if the scattering length  $a_s$  is larger than a critical value, equal to the dipolar length  $a_{\text{dd}}$  (white region in Fig. 3 (a)). Instability can instead occur if  $a_{\text{dd}} > a_s$ , as in this case dipolar attraction can dominate and drive the instability. For  $\epsilon_{\text{dd}} \approx 1$ , the instability occurs for  $\alpha_{\text{crit}} \approx \pi/2$ , corresponding to a dipole orientation nearly colinear with the atomic plane. This configuration maximizes the attractive contribution of the DDI and is therefore the most unstable. When  $\epsilon_{\text{dd}}$  increases we observe that  $\alpha_{\text{crit}}$  decreases. This is explained as less attraction is required to make the gas unstable. The instability for  $\alpha > \alpha_{\text{crit}}$  is justified as this corresponds to a larger attractive contribution of the DDI.

Figure 3 (a) also illustrates the density dependence of  $\alpha_{\text{crit}}$ . We observe that as the 2D density increases,  $\alpha_{\text{crit}}$  decreases. This effect relates to the fact that, in our settings, the instability is so-called local, driven by a finite momentum excitation, see Fig. 3 (b) and e.g. [1]. For such a local instability, a competition between the kinetic term  $\frac{\hbar^2 \mathbf{k}^2}{2m}$  and the total interaction which scales with the density as  $2n_0 \tilde{U}(\mathbf{k})$  comes into play, and lowering the density stabilizes the system through kinetic energy cost. The high-density states are more unstable and in Fig. 3, we can even observe that at very large density above  $10^{15}$  atoms/m<sup>2</sup> and small s-wave scattering length, the atomic cloud is unstable even at  $\alpha = 0$ .

In Fig. 3 (b), we further report on the norm of the most unstable wavevector  $\mathbf{q}_c$ , i.e. for which  $E_1(\mathbf{q}_c) = 0$  at  $\alpha = \alpha_{\text{crit}}$ . First of all, we note that at  $\alpha = \alpha_{\text{crit}}$ , the most unstable  $\mathbf{q}$  always corresponds to  $\phi = 0$ , that is to say that it is orthogonal to the dipole plane. The value of  $q_c$  allows regimes of global and local instabilities to be told apart, as respectively corresponding to  $q_c = 0$  and  $q_c \neq 0$ . The two regimes are separated by the green line in Fig. 3 (b), with the left side (low density, small  $\epsilon_{\text{dd}}$ ) corresponding to globally unstable cases. In the local instability regime, the value of  $q_c$  increases with increasing density and  $\epsilon_{\text{dd}}$ , taking values up to 1.75, meaning  $k \approx 2.5/l_z$ .

In dipolar gases, the mean-field instability is known to be overruled by beyond-mean-field effects, at least in some regimes [1]. Yet, here we do not consider this effect and restrict to a mean-field treatment of our gas (see Eq. (14)). In the following, we thus focus on the mean-field stable regime, meaning that for a set of density and scattering length values, we consider only angles with  $\alpha < \alpha_{\text{crit}}$ .

### III. DENSITY PERTURBATIONS FOR POTENTIAL DEFECTS OF FIXED MOMENTA

We now consider the effect of defects of the potential on the condensate density in the mean-field stable

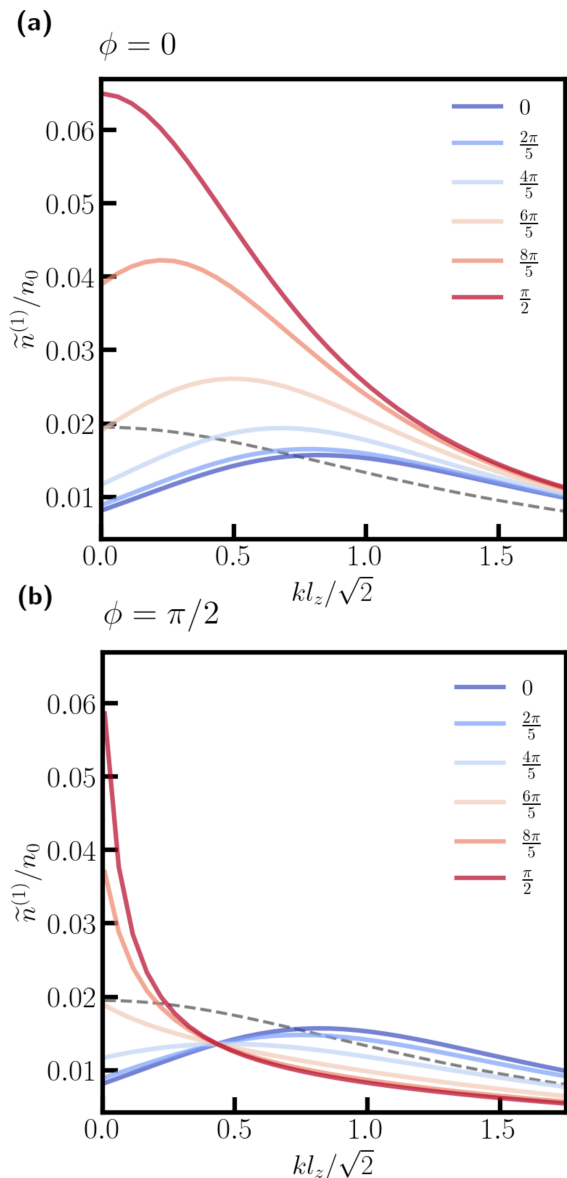


FIG. 4. **Density perturbation for varying angle  $\alpha$ .** Relative amplitude of the density perturbation  $\tilde{n}^{(1)}/n_0$  for a pure cosinusoidal perturbation of the potential  $\delta V = \delta V_0 \cos(\mathbf{k} \cdot \mathbf{r})$  with an amplitude  $\delta V_0$  of 1% of the trap depth  $V_0 = k_B \times 100$  nK. We set  $m = 164$  a.u.,  $a_s = 130 a_0$ ,  $n_0 = 125 \mu\text{m}^{-2}$ ,  $\nu_z = 1$  kHz, and  $\epsilon_{\text{dd}} = 0.7$ . Each curve is labeled by the value of the angle  $\alpha$  of the dipoles with the  $z$  axis, see legend. The gray dotted curve is calculated with the same parameters but in the pure contact case,  $\epsilon_{\text{dd}} = 0$ . (a) is for a perturbation along the  $y$  direction, orthogonal to the dipoles ( $\phi = 0$ ), and (b) for a perturbation along  $x$  ( $\phi = \pi/2$ ).

regime and in first order of perturbation theory, based on Eq. (14). First, we consider the effect of a pure cosinusoidal perturbation of the potential  $\delta V = \delta V_0 \cos(\mathbf{k} \cdot \mathbf{r})$  with wavevector  $\mathbf{k}$ . The gas' density perturbation is also cosinusoidal and its amplitude is given by  $\tilde{n}^{(1)}(\mathbf{k})$  (Eq. (14)) which depends on the norm of the wavevector

$k$  and of the angle of excitation direction  $\phi$ .

In the non-dipolar case  $\tilde{U}(\mathbf{k}) = g/\sqrt{2\pi\ell_z}$  such that  $\tilde{n}^{(1)}(\mathbf{k})$  is independent on  $\phi$  and is a Lorentzian in  $k$  with a maximum at  $k = 0$  and a characteristic momentum width given by that associated with the healing length. Adding dipolar interactions modifies  $\tilde{n}^{(1)}(\mathbf{k})$  in a non-trivial way (see Eq. (3)). Yet, using Eqs. (9)-(10), we find that the perturbation effects at  $k = 0$  and  $k \rightarrow \infty$  behave similarly to the pure contact case. At  $k = 0$ ,  $\tilde{n}^{(1)}$  has a finite amplitude independent of  $\phi$ . In the large  $k$  limit,  $\tilde{n}^{(1)}$  vanishes quadratically in  $k$  as the kinetic term dominates in the denominator of Eq. (14). The dipolar effects thus reveal at small but finite values of  $k$ .

We here study the strength of this density perturbation as a function of  $k$  and for different  $\phi$  in the dipolar case. To investigate the impact of the long-range and anisotropic character of the dipolar interactions, we control the angle of the dipoles,  $\alpha$ , compared to the atomic plane and the relative strength of the dipolar and contact interactions,  $\epsilon_{\text{dd}}$ . We also explore the influence of the gas parameters, namely its mean density and confinement strength. In the following, to vary  $\epsilon_{\text{dd}} = a_{\text{dd}}/a_s$ , we keep  $a_s$  fixed and vary  $a_{\text{dd}}$ . We note that this differs from the typical experimental situation where  $a_{\text{dd}}$  is a constant given by the atomic species and  $a_s$  can be easily varied by exploiting Feshbach resonances. The present choice is yet a sensible theoretical choice that allows a simplified comparison of different situations. We take  $a_s = 130 a_0$  such that the situation  $\epsilon_{\text{dd}} = 1$  matches the case of dysprosium atoms.

### A. Angular dependence of the perturbation

In a first study, we aim to reveal the effect of anisotropic long-range interaction on the behavior of the density perturbation  $\tilde{n}^{(1)}$ . In this aim, we explore the dependence of  $\tilde{n}^{(1)}(k)$  with the orientation of the dipoles and the excitation direction. Figure 4 shows the relative strength of the density perturbation as a function of  $k$  for various values of  $\alpha$  and for  $\phi = 0$  (a) and  $\phi = \pi/2$  (b) at fixed  $\epsilon_{\text{dd}} = 0.7$ .

A first stringent effect of the dipoles is evidenced through the qualitative change of the general  $k$ -dependent shape of the density perturbation when varying  $\alpha$ : While for dipoles nearly in the atomic plane ( $\alpha \sim \pi/2$ ), the perturbation is maximum at  $k = 0$  and strictly decreasing with  $k$  similar to the pure contact case, for dipoles nearly perpendicular to the atomic plane ( $\alpha \sim 0$ ),  $\tilde{n}^{(1)}$  is non-monotonous and have a maximum at a non-zero momentum,  $k_m$ . The two behaviors can be observed for both directions of excitations. The non-monotonous behavior connects to the existence of a minimum in Eq. (15), which was discussed in Sec. II C and Fig. 2. Briefly, the minimum occurs through the competition of the kinetic energy and an interaction contribution that decreases with  $k$  (long-range attraction). It is indicative of the potential softening of a roton mode

in the dispersion relation Eq. (16) yet it is present on a much broader range of parameters.

The transition between these two distinct behaviors as well as the position and amplitude of the maximum when it exists depends strongly on the gas and excitation parameters, see also later discussion in III D and Fig. 7. In Fig. 4 (a) and (b), a general trend can be observed with a shift of the maximum of the perturbation to lower wavenumber as  $\alpha$  increases. We also observe that the local maximum persists to larger values of  $\alpha$  for  $\phi = 0$  (a) than for  $\phi = \pi/2$  (b).

Comparing Fig. 4 (a) and (b) allows us to further highlight the anisotropic effect of the dipolar interactions. Indeed, except for the case  $\alpha = 0$ , strong discrepancies can be observed between the two perturbation directions, and the larger  $\alpha$ , the more obvious the discrepancy is. We observe that the density perturbation is always larger in the case  $\phi = 0$  (excitation perpendicular to the plane of the dipoles see Fig. 1 (a)) than in the case  $\phi = \pi/2$  (excitation in the plane of the dipoles). These observations connect to the additional repulsive contribution  $\propto \sin^2 \alpha \sin^2 \phi$  in the momentum-dependent interaction contribution Eq. (7) (second line).

In the case of  $\phi = \pi/2$  we observe a distinct behavior of the perturbation with  $\alpha$  for given  $k$  values: while the density perturbation increases with increasing  $\alpha$  for small  $k$ , the behavior with  $\alpha$  is inverted for large  $k$ . The value of the momentum at which the change of behavior occurs,  $k_*$  is remarkably independent on  $\alpha$  (all curves intercepts at the same  $k = k_*$ ). This can be understood from Eq. (8) where the  $\alpha$ -dependent contribution is isolated in the second line as  $\cos^2 \alpha (3 - f(q)(\sin^2 \phi + 1))$ . This contribution is repulsive at small  $k$ , attractive at large  $k$  and changes sign for  $q_*$  solution of  $f(q_*) = \frac{3}{(\sin^2 \phi + 1)}$  independent on  $\alpha$ . For  $\phi = 0$ , this gives  $f(q_*) = 3$ , which corresponds to  $q_* \rightarrow \infty$  if you look at Fig. 1: Increasing the angle  $\alpha$  will always lead to a larger perturbation. For  $\phi = \pi/2$  (excitation in the plane of the dipoles),  $q_*$  is of order 0.5 and so corresponds to a momentum of the order of  $1/\ell_z$ . The change of behavior with  $\alpha$  is thus understood as a length-scale competition for which direction limits the attractive contribution of the dipolar interactions. The behavior at small  $k$  matches the dependence of the in-plane mean interaction energy (see chemical potential  $\mu$ , Eq. (11)), which decreases when increasing  $\alpha$  due to the increased dipolar attraction in plane. At  $k > k_*$ , the density modulation has a length scale smaller than the typical vertical size of the atomic cloud and the interactions along  $z$  become relevant, thus inverting the dependence with  $\alpha$ .

### B. Effects of the relative strength of contact and dipolar interactions

While the analysis of the angular dependence allowed us to directly highlight the impact of dipolar interactions and its anisotropic effect, another important parameter

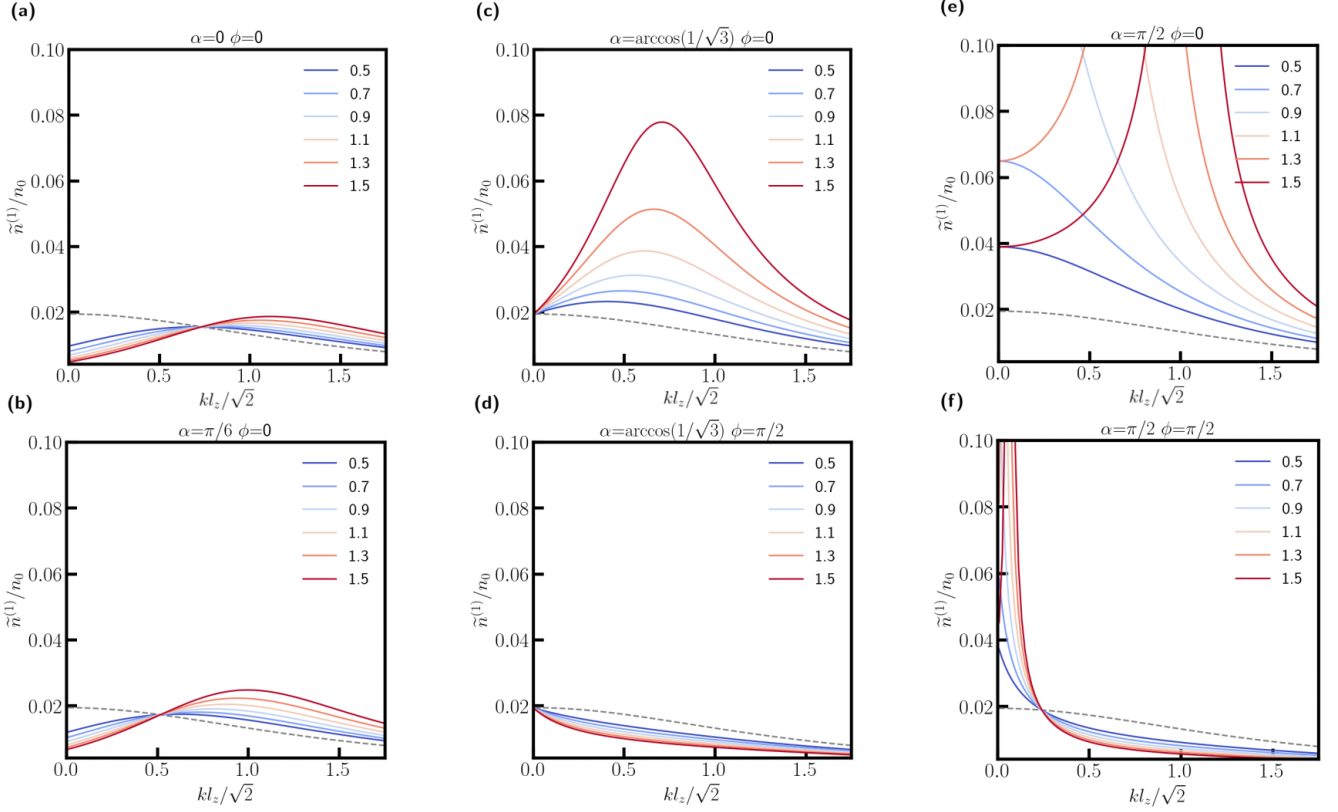


FIG. 5. **Density perturbation for varying  $\epsilon_{\text{dd}}$ .** Relative amplitude of the density perturbation,  $\tilde{n}^{(1)}/n_0$  for a pure cosinusoidal perturbation of the potential  $\delta V = \delta V_0 \cos(\mathbf{k} \cdot \mathbf{r})$  with an amplitude  $\delta V_0$  of 1% of the trap depth  $V_0 = k_B \times 100 \text{ nK}$ . We take  $m = 164 \text{ a.u.}$ ,  $n_0 = 125 \mu\text{m}^{-2}$ ,  $\nu_z = 1 \text{ kHz}$  and  $a_s = 130 a_0$ , while  $\epsilon_{\text{dd}}$  is changed by tuning the value of  $a_{\text{dd}}$ . Each curve is labeled by the value of  $\epsilon_{\text{dd}}$  (legend). The gray dotted curve is calculated with the same parameters but in the pure contact case,  $\epsilon_{\text{dd}} = 0$ . Each panel is for a different set of angles, see panel title.

that regulates the role of the dipolar interaction is its relative strength with respect to the contact interaction, encompassed by the parameter  $\epsilon_{\text{dd}}$ . Studying the impact of  $\epsilon_{\text{dd}}$  on the strength of the density perturbation is of high relevance as this parameter is usually tuned in experiments to enhance dipolar effects, see e.g. [1]. We investigate this effect in Fig. 5 where the strength of the density perturbation as a function of  $k$  is shown for varying  $\epsilon_{\text{dd}}$  and showcased for different values of the angles  $(\phi, \alpha)$ .

The panels 5 (a,b) focus on the case of small  $\alpha$ , i.e. dipoles nearly perpendicular to the atomic plane, and  $\phi = 0$ . They display similar behaviors: for small momenta, the strength of the perturbation decreases with increasing dipolar interaction strength (increasing  $\epsilon_{\text{dd}}$ ); for momenta larger than a critical value,  $k'_*$ , the behavior is inverted with increasing perturbation for increasing dipolar strength. The value of  $k'_*$  is independent of  $\epsilon_{\text{dd}}$  and corresponds to the value of  $q$  where  $F(\mathbf{q}, \alpha)$  changes of sign, see Eq. (7). The behavior of  $F(\mathbf{q}, \alpha)$  yields a repulsive contribution of the DDI at small  $k$  and an attractive one at large  $k$ . The repulsive contribution reduces the perturbation while the attractive one amplifies

it. As increasing  $\alpha$  increases the mean ( $k = 0$ ) attractive DDI contribution,  $k'_*$  is shifted to lower values and the strength of the perturbation is increased. We note that while at  $\alpha = 0$ , the behavior is independent of the excitation direction  $\phi$ , at finite  $\alpha$  anisotropic behaviors occur and  $k'_*$  depends on  $\phi$ , see Eq. (7).

The panels 5(c,d) illustrate a larger tilt of the dipoles, at the so-called magic angle  $\alpha_m = \arccos(1/\sqrt{3})$  and for two different directions of excitations  $\phi = 0$  (c) and  $\phi = \pi/2$  (d). At this angle,  $k'_*$  is shifted to zero frequency for all excitation directions, as visible in these figure panels. The different excitation directions translate into different behaviors of the perturbation at finite  $k$ : first, the perturbation is much stronger for  $\phi = 0$  (perturbation perpendicular to the dipole plane) than for  $\phi = \pi/2$  (perturbation in the dipole plane) at all  $k$  connecting to the observation of Fig. 4; second, for  $\phi = 0$  the perturbation strength increases for increasing  $\epsilon_{\text{dd}}$  at all finite  $k$  matching the observations of 5 (a,b), while for  $\phi = \pi/2$  this relation is inverted and the perturbation decreases for increasing  $\epsilon_{\text{dd}}$ . This behavior relates to the sign of the dipolar contribution being respectively attractive or repulsive at finite  $k$ , see second line of Eq. (7). We note

that for the case  $\alpha = \alpha_m$  and  $\phi = \pi/4$ ,  $F(\mathbf{q}, \alpha)$  vanishes for all  $\mathbf{q}$  and hence there is no dipolar effect in the density perturbation.

Finally, the panels 5 (e,f), illustrate the case of the dipoles being in the 2D plane. In this case, the dipolar interaction is attractive along  $x$  and if the dipolar interactions dominate, i.e.  $\epsilon_{dd} > 1$ , the system becomes unstable, see also Fig. 3. This manifests through divergences of  $\tilde{n}^{(1)}$  at finite values of the momenta for  $\epsilon_{dd} \geq 1$ . As observed previously, the strength of the perturbation is stronger for  $\phi = 0$  than for  $\phi = \pi/2$  and the divergences occur first in the former case, as observed in Fig. 5 (e). Here we additionally see that the unstable momentum region shifts to larger momenta for increasing  $\epsilon_{dd}$ , see also Fig. 3 (b). For  $\epsilon_{dd}$  approaching 1 from below,  $\tilde{n}^{(1)}$  becomes very large at some specific values of the momentum, close to the instability momentum. In this case, the presence of a small perturbation may lead to strong perturbations of the density distribution, breaking the perturbation regime relevant in the present work and reminiscent of the emergence of spontaneous density modulation (e.g. supersolid states) in such systems, see e.g. ref. [1] and discussion above. In the case  $\phi = \pi/2$ , we observe that the perturbation strength increases at  $k < k'_*$  and may diverge in the case  $\epsilon_{dd} > 1$  but it decreases at  $k > k'_*$  for increasing  $\epsilon_{dd}$ . This behavior leads to strongly attenuated density perturbation for  $\phi = \pi/2$  compared to  $\phi = 0$  at large  $k$ . This change of behavior is reminiscent of our observation in Fig. 5 (a) yet with an inverted trend, similar to the inversion discussed in Fig. 5 (d). In the case  $\phi = 0$ , we observe instead that the perturbation strength increases at large  $k$  for increasing  $\epsilon_{dd}$ . This relation extends to small  $k$  for  $\epsilon_{dd} < 1$  similar to Fig. 5 (c), yet no univocal relationship holds at small  $k$  and  $\epsilon_{dd} \geq 1$ .

### C. Impact of the gas parameters

Besides the parameters of the interaction itself, the development of the density perturbation is also influenced by the gas parameters, in particular its mean density and its confinement strength, which are also of experimental relevance. Not only do these two parameters come into play as rescaling parameters for the density perturbation ( $\tilde{n}^{(1)}/n_0$ ) and for the momenta ( $q = k\ell_z/\sqrt{2}$ ), but they also fundamentally dictate the competition between kinetic and interaction terms at play in Eq. (15). Indeed, using Eqs. (3) and (15), we see that the strength of the interaction terms scales linearly with  $n_0^{(3D)} = n_0/\sqrt{2\pi}l_z$ , which effectively matches the 3D density of the gas. We note that the effect of  $1/l_z$  is yet not fully equivalent to that of  $n_0$  as  $l_z$  rescales the momentum dependence of the interaction but not of the kinetic term therefore influencing further the competition of the two terms. In Fig. 6, we explore the effects of  $n_0^{(3D)}$  and  $l_z$  on the density perturbation under cosinusoidal potential defects.

Figure 6 (a) shows the perturbation strength as a func-

tion of  $k$  for different mean atomic 3D densities  $n_0^{(3D)}$  in the case  $\alpha = 0$  and large  $\epsilon_{dd}$ . For all densities, we observe the same shape as in Fig. 5(a), with a maximum at a finite  $k = k_m$ . We observe that  $k_m$  shifts to larger values for increasing density. The amplitude of the maximum itself first decreases and then increases with density. The underlying change of trend in the density perturbation strength seems to visually match the density for which  $k_m$  crosses the momentum where all the curves meet,  $k_*''$ . This intersection point  $k_*''$  corresponds to a momentum at which the density perturbation is insensitive to change in the mean density, which according to Eq. (14), occurs when the dipolar and contact interactions compensate each other such that  $\tilde{U}(k_*'') = 0$ . For  $k < k_*''$ , the interactions are repulsive, and increasing the density increases the strength of this repulsion and thus reduces the perturbation strength. Instead for  $k > k_*''$ , the interactions are attractive and the opposite behavior is found. Furthermore, we note that when the dipoles are tilted ( $\alpha > 0$ ),  $k_*''$  shifts toward smaller values and the perturbation becomes larger, and increasing  $\phi$  shifts this point toward larger values and decreases the density perturbation. We can even reach a case where this intersection point seems to no longer exist even at large  $q$  as in Fig. 6 (b) and where increasing the density always reduces the perturbation.

In Figure 6 (c), we now fix the 3D density  $n_0^{(3D)}$  and vary  $l_z$  in the case  $\alpha = 0$  and large  $\epsilon_{dd}$  as in Figure 6 (a). We here report the variation of the density perturbation as a function of the dimensioned momentum  $k$ . This choice show that  $l_z$  has actually only a small effect on the position of the maximum of the perturbation  $k_m$ : when the trapping frequency decreases for a fixed  $n_0^{(3D)}$ ,  $k_m$  shifts to lower values only by a small amount. The effects of  $l_z$  on the dimensionless momentum  $q$  and 2D density seem to compensate one another. A decrease of  $\nu_z$  is also associated with an increase of the perturbation similar to what was observed when changing  $n_0^{(3D)}$  in Fig. 6 (a,b) as it yields a decrease of the 2D density  $n_0$ .

### D. Momentum of the density perturbation maximum

In the previous subsections, it was found that a special feature arising from the dipolar character of the interaction is a non-monotonous dependence of the density perturbation strength with the momentum of the perturbation, for some regime of the parameters. This non-monotonous behavior yields strong density perturbations for defects of spatial wavenumber in the vicinity of  $k_m$ , the maximum, and its characterization is therefore crucial to apprehend the density perturbation arising from potential defects in dipolar gases. As discussed in Sec. III A, the position and amplitude maximum markedly depend on the gas and excitation parameters. In the present subsection, we quantitatively analyze how the momentum at which this maximum oc-



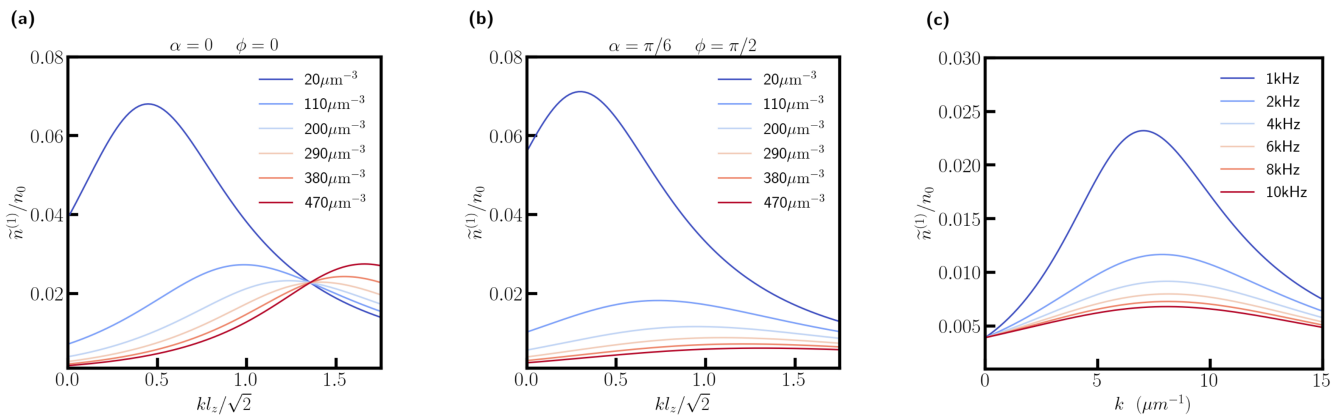


FIG. 6. **Density perturbation for varying  $n_0$  and  $l_z$ .** Relative amplitude of the density perturbation,  $\tilde{n}^{(1)}/n_0$  for a pure cosinusoidal perturbation of the potential  $\delta V = \delta V_0 \cos(\mathbf{k} \cdot \mathbf{r})$  with an amplitude  $\delta V_0$  of 1% of the trap depth  $V_0 = k_B \times 100$  nK. We take  $m = 164$  a.u.,  $a_s = 130a_0$ ,  $\epsilon_{\text{dd}} = 2$ . In panels (a,b), the trapping frequency is fixed at  $\nu_z = 1$  kHz and the curves are labeled by the value of the 3D density  $n_0^{(3D)}$  (legend). The two panels differ by the values of  $(\alpha, \phi)$ , see titles. In panel (c), the 3D atomic density is fixed to  $n_0^{(3D)} = 200 \mu\text{m}^{-3}$ ,  $\alpha = \phi = 0$ , and the curves are labeled by the value of  $\nu_z$  (legend).

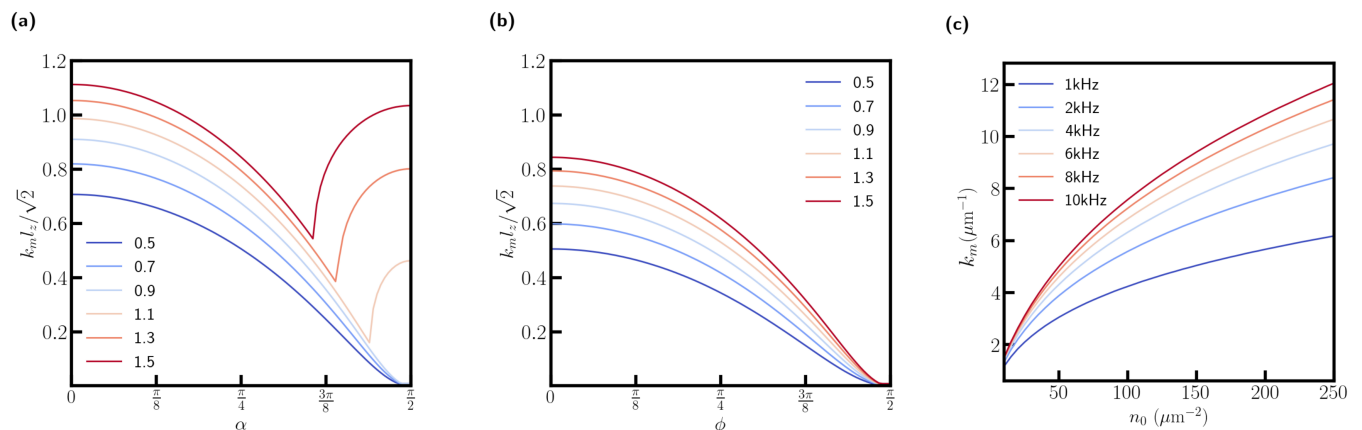


FIG. 7. **Momentum  $k_m$  of the density perturbation maximum for varying gas and interaction parameters.** (a)  $k_m$  for  $\phi = 0$  and varying  $\alpha$ . (b)  $k_m$  for  $\alpha = \pi/4$  and varying  $\phi$ . In (a) and (b), the curves are labeled by the value of  $\epsilon_{\text{dd}}$ , and  $k_m$  is plotted in its dimensionless form  $k_m l_z / \sqrt{2}$  using  $n_0 = 125 \mu\text{m}^{-2}$  and  $\nu_z = 1$  kHz. (c)  $k_m$  for  $\alpha = \phi = 0$ ,  $\epsilon_{\text{dd}} = 0.7$  and varying  $n_0$ , the curves being labeled by the value of  $\nu_z$ . The other parameters are  $m = 164$  a.u.,  $a_s = 130 a_0$ ,  $\delta V_0$  of 1% of the trap depth  $V_0 = k_B \times 100$  nK.

curs,  $k_m$ , evolves with the different parameters, namely the angles  $\alpha$  and  $\phi$ , and the parameters  $\epsilon_{\text{dd}}$ ,  $n_0$ ,  $l_z$ .

Figure 7 (a) shows the evolution of  $k_m$  as a function of  $\alpha$  and for different  $\epsilon_{\text{dd}}$ . For  $\epsilon_{\text{dd}} < 1$ ,  $k_m$  decreases with increasing  $\alpha$  as already reported when describing Fig. 4. As explained earlier, the maximum occurs when the momentum-dependence induced by dipolar interaction is attractive and strong enough to compete with the kinetic contribution, see second line in Eq. (7) and Eq. (15). Increasing  $\alpha$  makes the dipolar contribution along  $x$  more and more attractive and along  $z$  more and more repulsive. This reduces the interaction contribution at small momenta and increases that at large momenta depending on the sign of  $3 - f(q)[\sin^2 \phi + 1]$  in Eq. (8). This weakens the momentum dependence of the interac-

tion as visible in Fig. 2 and therefore shifts its competition with the kinetic energy to lower momenta. We also observe that  $k_m$  increases with  $\epsilon_{\text{dd}}$  for all  $\alpha$ . This is because increasing  $\epsilon_{\text{dd}}$  increases the overall strength of the momentum-dependent interaction and shifts its competition with the kinetic term to large momenta. For  $\epsilon_{\text{dd}} > 1$  we observe a non-monotonous behavior of  $k_m$  with  $\alpha$  as already observed when describing Fig. 5(e). The change of behavior reveals the occurrence of a mean-field instability and the critical angle for this instability, see also Fig. 3.

Figure 7 (b) reports on the evolution of  $k_m$  as a function of the excitation direction for different  $\epsilon_{\text{dd}}$  in the case  $\alpha = \pi/4$ . We observe that  $k_m$  decreases from a finite value at  $\phi = 0$  (excitation perpendicular to the dipole

plane) to  $k_m = 0$  at  $\phi = \pi/2$  (excitation in the dipole plane). The decrease of  $k_m$  results from the reduction of momentum-dependent dipolar attraction when making the excitation more and more along the dipoles, as encompassed by the second line of Eq. (7). As mentioned above this increases the dipolar attraction at small momenta and reduces that at small momenta. In the studied angular configuration, a contact-like monotonous behavior of  $\tilde{n}^{(1)}$  is recovered at  $\phi = \pi/2$ , as the momentum dependence cancels in Eq. (7) (note that we have exact cancellation only in the case  $\alpha = \pi/4$ ).

Finally, Figure 7 (c) reports on the evolution of  $k_m$  as a function of the gas density for different transverse  $\nu_z$ . Increasing  $n_0$  and  $\nu_z$  both lead to shifting  $k_m$  to larger values. Similar to the evolution with  $\epsilon_{dd}$ , this is because such an increase favors the interaction terms in its competition with the kinetic term.

Based on this analysis, we see that perturbations in the potential can lead to enhanced density fluctuations on certain length scales, the values of which  $\approx 2\pi/k_m$  shift with both the interaction and the gas parameters in dipolar systems. This can be detrimental because deviations from the uniform case occur differently in different experimental conditions, but it can also be used to one's advantage to make the system response parameter-dependent and e.g. to induce pattern formation in gases.

#### IV. DENSITY PERTURBATIONS FOR WHITE NOISE POTENTIAL DEFECTS

Now that we have understood the effects of the different Fourier components of the potential defects on the density perturbations individually, we are interested in this last part in studying density perturbations induced by more complex and realistic potential perturbation. Here we will focus on the relevant case of random potentials. In this aim, we consider a flat potential of depth  $V_0 = k_B \times 100$  nK perturbed by white noise including all momenta of wavenumber in the range  $[k_{\min}, k_{\max}]$  with an amplitude such that the standard deviation of the potential obtained is of  $k_B \times 1$  nK. We choose  $k_{\min} = 0.06$  rad/ $\mu\text{m}$  corresponding to a 100- $\mu\text{m}$ -wide defect, on the order of a typical size of uniform trap in cold atom experiments, and  $k_{\max} = 13$  rad/ $\mu\text{m}$  corresponding to a 500-nm-wide defect roughly the size of the wavelength of the light used to generate the optical trap. We obtain the perturbed density by calculating the inverse Fourier transform of Eq. (14), and summing over all momentum components. The result is then averaged over 20 realizations of white noise potential, where the phase of each momentum component of the potential defect are randomly drawn following a uniform distribution. Our numerical calculation uses a momentum discretization with steps of  $\delta k = 2\pi \times 10^{-2}$   $\mu\text{m}^{-1}$ . We examine the dependence of the maximal amplitude of the resulting density perturbation,  $n_1$  as a function of the different parameters  $(\alpha, \epsilon_{dd}, n_0, l_z)$ . We define  $n_1 = n_{\max} - n_{\min}$ ,

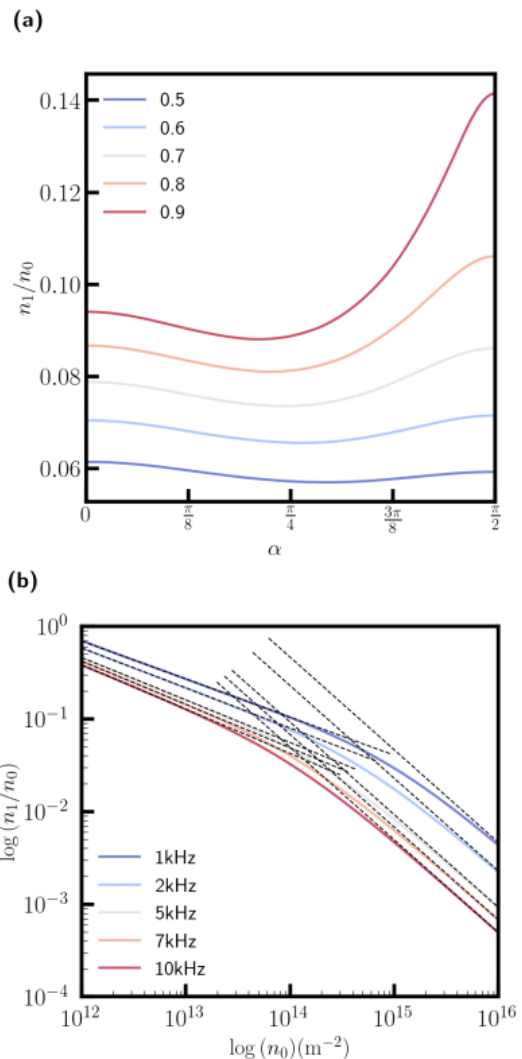


FIG. 8. **Density perturbation in white noise potential.** Relative perturbation of the density around a uniform atomic cloud of density  $n_0 = 125\mu\text{m}^{-2}$  for a white noise perturbed potential with a standard deviation of  $k_B \times 1$  nK. We set  $m = 164$  a.u.,  $a_{dd} = 133 a_0$ . The perturbation  $n_1$  is the amplitude of the variation of the density over the trap  $n_1 = n_{\max} - n_{\min}$ . (a)  $n_1$  as a function of  $\alpha$ , with  $\nu_z = 1$  kHz. The different curves are labeled by the value of  $\epsilon_{dd}$  (legend). (b)  $n_1$  plotted in a log-log scale as a function of the background density  $n_0$ . The different curves are labeled by the value of  $\nu_z$  (legend). The black dotted lines are linear fit of the values at high density  $n_0 > 10n_{0c}$  and low densities  $n_0 < 0.1n_{0c}$  (see text). The other parameters used are  $a_s = 150a_0$  and  $\alpha = 0$ .

where  $n_{\max(\min)}$  are the minimum and maximum of the perturbed gas density, respectively. The results are summarized in Fig. 8.

Figure 8 (a) shows the amplitude of the density perturbation as a function of the dipole angle  $\alpha$  and for various values of  $\epsilon_{dd}$ . We keep  $\epsilon_{dd} < 1$  to avoid instabilities (see Sec. IID). For all values of  $\epsilon_{dd}$ , we observe a similar non-monotonous evolution of  $n_1$  with  $\alpha$ , where  $n_1$  first

decreases and then increases with increasing  $\alpha$ . The position of the minimum in  $n_1$  shifts to smaller angle with increasing  $\epsilon_{\text{dd}}$ , being at  $\alpha = 0.3\pi$  for  $\epsilon_{\text{dd}} = 0.5$  and at  $\alpha = 0.217\pi$  for  $\epsilon_{\text{dd}} = 0.9$ . We also observe a strong impact of the value of  $\epsilon_{\text{dd}}$  on the amplitude of  $n_1$ . Increasing  $\epsilon_{\text{dd}}$  leads to overall larger values of  $n_1$  with the sharper increase being found for  $\alpha \simeq \pi/2$  when  $\epsilon_{\text{dd}} \rightarrow 1$ , which evidences the tendency toward the instability discussed earlier, see Fig. 3.

Figure 8 (b) reports on the effect of the gas parameters, showing the amplitude of the density perturbation as a function of the mean density  $n_0$  and for different confinement strength  $\nu_z$ . The dependence of the perturbation on the mean density  $n_0$  is plotted in log-log scale, which evidences two distinct regimes, holding respectively at high and low densities. In both cases, we observe a power scaling that appears to hold with similar power for all values of  $\nu_z$ . Fits of the calculated  $\frac{n_1}{n_0}$  to  $n_0^{-\gamma}$  for different values of  $\nu_z$  yield  $\gamma = 0.45 \pm 0.02$  and  $\gamma = 1 \pm 10^{-5}$  at small and large densities respectively.

The different behaviors as a function of  $n_0$  can be related to the functional form of Eq. (15). Here the density-independent kinetic and the density-dependent interaction terms compete. Depending on the density regime, one term dominates the other and different behaviors are expected. The density  $n_{0c}$  at which the kinetic and the interaction terms are of the same order of magnitude for the range of momenta  $[k_{\text{min}}, k_{\text{max}}]$  separates the two regimes. In a first approximation,  $n_{0c}$  is given by  $n_{0c}(\nu_z) \sim \frac{k_{\text{max}}^2 \nu_z}{8\sqrt{2}\pi a_s}$ . For  $n_0 < n_{0c}$ , the kinetic effects dominate, and, in the case where the interactions can be neglected for all  $k$ , no density dependence of  $\frac{\tilde{n}^{(1)}(\mathbf{k})}{n_0}$  would be expected. The observed power law of  $\tilde{n}^{(1)}(\mathbf{k}) \sim n_0^{0.55}$  evidences residual effects of interaction in the considered density range. For  $n_0 > n_{0c}$ , the interaction effects dominate and one expect  $\frac{\tilde{n}^{(1)}(\mathbf{k})}{n_0} \simeq \frac{-\delta\tilde{V}(\mathbf{k})}{n_0\tilde{U}(\mathbf{k})}$  matching well the observed power law. We note that the high-density scaling yields a perturbation  $n_1$  independent of the background density  $n_0$ .

## V. CONCLUSIONS AND PERSPECTIVES

In this paper, we investigated the density perturbations of a quasi-two-dimensional dipolar Bose gas in perturbed potentials within mean-field theory. We recovered the usual mean-field instability [1, 24, 27, 30, 31] when the dipolar interaction strength is larger than the contact one. We studied the dependence of the density perturbation on the wavevector of the perturbing potential and on different gas and interaction parameters, including the orientation of the dipoles. The anisotropy of the dipole

interaction gives rise to angular dependences, and its long-range character translates into effects at intermediate momenta. For a wide range of parameters, the perturbation exhibits a maximum at a finite wavenumber whose value varies with the gas parameters. These variations may allow to mitigate density perturbations in a perturbed trap by tuning the gas parameters. Finally, we studied the density in a more realistic randomly perturbed trap, and found that at high densities the density perturbation is independent of the background density.

Our work explores the possibility of realizing dipolar quantum gases confined in uniform potentials. It sheds light on the effect of unavoidable potential imperfections, e.g. due to optical aberrations on the dipole trapping beam. It highlights the challenge of realizing homogeneous dipolar gases over a wide range of gas parameters, but also the possibility of mitigating the potential imperfections by careful choice of gas parameters. Here we have considered first-order perturbations in the mean-field approximation. This can be extended to the second order as in [18–23] where a condensate depletion is predicted. A natural and intriguing extension of the present work is to address the regime of mean-field instability, which could be done, for example, by including beyond mean-field stabilization of the condensate. In this case, the intriguing effects of potential defects (involuntary or voluntary) on self-organized ground states are to be discussed [1].

## ACKNOWLEDGMENTS

We thank Karthik Chandrashekar, Jianshun Gao, Shuwei Jin, Christian Götzhauser, Charles Drevon, Sarah Philips, Maurice Rieger and Britta Bader for insightful discussions. We thank Wyatt Kirkby for his careful reading and helpful comments on the manuscript. This work is funded by the European Research Council (ERC) under the European Union’s Horizon Europe research and innovation program under grant number 101040688 (project 2DDip), and by the Deutsche Forschungsgemeinschaft (DFG, German Research Foundation) through project-ID 273811115 (SFB1225 ISO-QUANT) and under Germany’s Excellence Strategy EXC2181/1-390900948 (the Heidelberg Excellence Cluster STRUCTURES). Views and opinions expressed are however those of the authors only and do not necessarily reflect those of the European Union or the European Research Council. Neither the European Union nor the granting authority can be held responsible for them.

★ Correspondence and requests for materials should be addressed to chomaz@uni-heidelberg.de.

[1] Lauriane Chomaz, Igor Ferrier-Barbut, Francesca Ferlaino, Bruno Laburthe-Tolra, Benjamin L Lev, and

Tilman Pfau, “Dipolar physics: a review of experiments

- with magnetic quantum gases,” *Reports on Progress in Physics* **86**, 026401 (2022).
- [2] H.-Y. Lu, H. Lu, J.-N. Zhang, R.-Z. Qiu, H. Pu, and S. Yi, “Spatial density oscillations in trapped dipolar condensates,” *Phys. Rev. A* **82**, 023622 (2010).
- [3] S. M. Rocuzzo, S. Stringari, and A. Recati, “Supersolid edge and bulk phases of a dipolar quantum gas in a box,” *Phys. Rev. Res.* **4**, 013086 (2022).
- [4] J. Hertkorn, J.-N. Schmidt, M. Guo, F. Böttcher, K. S. H. Ng, S. D. Graham, P. Uerlings, T. Langen, M. Zwierlein, and T. Pfau, “Pattern formation in quantum ferrofluids: From supersolids to superglasses,” *Phys. Rev. Res.* **3**, 033125 (2021).
- [5] Yong-Chang Zhang, Thomas Pohl, and Fabian Maucher, “Phases of supersolids in confined dipolar bose-einstein condensates,” *Phys. Rev. A* **104**, 013310 (2021).
- [6] L. Amico, M. Boshier, G. Birkel, A. Minguzzi, C. Miniatura, L.-C. Kwek, D. Aghamalyan, V. Ahufinger, D. Anderson, N. Andrei, A. S. Arnold, M. Baker, T. A. Bell, T. Bland, J. P. Brantut, D. Cassettari, W. J. Chetcuti, F. Chevy, R. Citro, S. De Palo, R. Dumke, M. Edwards, R. Folman, J. Fortagh, S. A. Gardiner, B. M. Garraway, G. Gauthier, A. Günther, T. Haug, C. Hufnagel, M. Keil, P. Ireland, M. Lebrat, W. Li, L. Longchambon, J. Mompert, O. Morsch, P. Naldesi, T. W. Neely, M. Olshanii, E. Orignac, S. Pandey, A. Pérez-Obiol, H. Perrin, L. Piroli, J. Polo, A. L. Pritchard, N. P. Proukakis, C. Rylands, H. Rubinsztein-Dunlop, F. Scazza, S. Stringari, F. Tosto, A. Trombettoni, N. Victorin, W. von Klitzing, D. Wilkowski, K. Khani, and A. Yaki-menko, “Roadmap on Atomtronics: State of the art and perspective,” *AVS Quantum Science* **3**, 039201 (2021), [https://pubs.aip.org/avs/aqs/article-pdf/doi/10.1116/5.0026178/16662758/039201\\_1\\_online.pdf](https://pubs.aip.org/avs/aqs/article-pdf/doi/10.1116/5.0026178/16662758/039201_1_online.pdf).
- [7] Péter Juhász, Milan Krstajić, David Strachan, Edward Gandar, and Robert P. Smith, “How to realize a homogeneous dipolar bose gas in the roton regime,” *Phys. Rev. A* **105**, L061301 (2022).
- [8] Matthew P. A. Fisher, Peter B. Weichman, G. Grinstein, and Daniel S. Fisher, “Boson localization and the superfluid-insulator transition,” *Phys. Rev. B* **40**, 546–570 (1989).
- [9] Kerson Huang and Hsin-Fei Meng, “Hard-sphere bose gas in random external potentials,” *Phys. Rev. Lett.* **69**, 644–647 (1992).
- [10] S. Giorgini, L. Pitaevskii, and S. Stringari, “Effects of disorder in a dilute bose gas,” *Phys. Rev. B* **49**, 12938–12944 (1994).
- [11] L. Sanchez-Palencia, “Smoothing effect and delocalization of interacting bose-einstein condensates in random potentials,” *Phys. Rev. A* **74**, 053625 (2006).
- [12] G. M. Falco, A. Pelster, and R. Graham, “Thermodynamics of a bose-einstein condensate with weak disorder,” *Phys. Rev. A* **75**, 063619 (2007).
- [13] Christopher Gaul and Cord A. Müller, “Bogoliubov excitations of disordered bose-einstein condensates,” *Phys. Rev. A* **83**, 063629 (2011).
- [14] Tama Khellil, Antun Balaž, and Axel Pelster, “Analytical and numerical study of dirty bosons in a quasi-one-dimensional harmonic trap,” *New Journal of Physics* **18**, 063003 (2016).
- [15] Tama Khellil and Axel Pelster, “Dirty bosons in a three-dimensional harmonic trap,” *Journal of Statistical Mechanics: Theory and Experiment* **2017**, 093108 (2017).
- [16] B. C. Crooker, B. Hebral, E. N. Smith, Y. Takano, and J. D. Reppy, “Superfluidity in a dilute bose gas,” *Phys. Rev. Lett.* **51**, 666–669 (1983).
- [17] Benjamin Nagler, Milan Radonjić, Sian Barbosa, Jennifer Koch, Axel Pelster, and Artur Widera, “Cloud shape of a molecular bose-einstein condensate in a disordered trap: a case study of the dirty boson problem,” *New Journal of Physics* **22**, 033021 (2020).
- [18] Christian Krumnow and Axel Pelster, “Dipolar bose-einstein condensates with weak disorder,” *Phys. Rev. A* **84**, 021608(R) (2011).
- [19] Branko Nikolić, Antun Balaž, and Axel Pelster, “Dipolar bose-einstein condensates in weak anisotropic disorder,” *Phys. Rev. A* **88**, 013624 (2013).
- [20] Mahmoud Ghabour and Axel Pelster, “Bogoliubov theory of dipolar bose gas in a weak random potential,” *Phys. Rev. A* **90**, 063636 (2014).
- [21] Abdelâali Boudjemâa, “Dipolar bose gas in a weak isotropic speckle disorder,” *Phys. Rev. A* **91**, 053619 (2015).
- [22] Abdelâali Boudjemâa, “Two-dimensional dipolar bosons with weak disorder,” *Physics Letters A* **379**, 2484–2487 (2015).
- [23] Abdelâali Boudjemâa, “Thermodynamics of a two-dimensional dipolar bose gas with correlated disorder in the roton regime,” *Journal of Physics B: Atomic, Molecular and Optical Physics* **49**, 105301 (2016).
- [24] Lev Pitaevskii and Sandro Stringari, *Bose-Einstein condensation and superfluidity*, Vol. 164 (Oxford University Press, 2016).
- [25] D. Baillie and P. B. Blakie, “Droplet crystal ground states of a dipolar bose gas,” *Phys. Rev. Lett.* **121**, 195301 (2018).
- [26] Christopher Ticknor, Ryan M. Wilson, and John L. Bohn, “Anisotropic superfluidity in a dipolar bose gas,” *Phys. Rev. Lett.* **106**, 065301 (2011).
- [27] Uwe R. Fischer, “Stability of quasi-two-dimensional bose-einstein condensates with dominant dipole-dipole interactions,” *Phys. Rev. A* **73**, 031602(R) (2006).
- [28] L. Santos, G. V. Shlyapnikov, and M. Lewenstein, “Roton-maxon spectrum and stability of trapped dipolar Bose-Einstein condensates,” *Phys. Rev. Lett.* **90**, 250403 (2003).
- [29] D. H. J. O’Dell, S. Giovanazzi, and G. Kurizki, “Rotons in gaseous bose-einstein condensates irradiated by a laser,” *Phys. Rev. Lett.* **90**, 110402 (2003).
- [30] N. G. Parker, C. Ticknor, A. M. Martin, and D. H. J. O’Dell, “Structure formation during the collapse of a dipolar atomic Bose-Einstein condensate,” *Phys. Rev. A* **79**, 013617 (2009).
- [31] J. L. Bohn, R. M. Wilson, and S. Ronen, “How does a dipolar Bose-Einstein condensate collapse?” *Laser Physics* **19**, 547–549 (2009).